Nuclear shell structure and rotational bands in ^{86}Nb

B. G. Carlsson and I. Ragnarsson
Division of Mathematical Physics, Lund Institute of Technology, P.O. Box 118, SE-221 00 Lund, Sweden
(Received 2 March 2004; published 13 August 2004)

The high spin structures in ^{86}Nb are analyzed using the cranked Nilsson-Strutinsky model. Energy versus spin curves as well as deformations and electric transition quadrupole moments are considered. It is concluded that different single-particle parameters compared with the standard values lead to better agreement with recent experimental results.

DOI: 10.1103/PhysRevC.70.024303 PACS number(s): 21.60.−n, 21.10.Ky, 21.10.Pc, 27.50.+e

I. INTRODUCTION

Configuration dependent cranked Nilsson-Strutinsky calculations with the modified oscillator potential have been very successful in describing high-spin rotational bands in different regions of the nuclear periodic table. The best examples are found in nuclei with a few particles outside closed shells where it has been possible to describe many bands up to their maximum spin values with a surprising accuracy [1]. These bands are generally built in the valence space but often with one or a few holes in the core. Furthermore a good understanding of superdeformed bands in different regions have been obtained using this model, see, e.g., [2–4]. One region where this model has met some difficulties is, however, nuclei with holes in a ^{100}Sn core, i.e., nuclei with the proton as well as neutron valence space in the upper part of the $N=3$ shell and in the $g_{9/2}$ subshell. One specific case is ^{87}Nb where calculations tend to give rotational bands which terminate much more favored in energy, i.e., the bands slope more downwards when drawn versus a standard $I(I+1)$ reference, than observed in experiment [5]. The problems became more apparent to us when we carried out calculations [6] for ^{86}Nb [7] where we noticed similar features as for ^{87}Nb. Problems of this kind are also seen for ^{86}Zr [8,9], even though the configurations of the observed bands appear to be better understood in this nucleus than in the Nb isotopes.

One specific feature of these bands in $A=86$, 87 nuclei is that they are generally calculated as oblate or close to oblate at intermediate and high spin values which can be understood from the fact that their configurations are most naturally described as holes in a core. Another difficulty is that the observed yrast line consists of many competing structures displaying a large variety of collective and single-particle degrees of freedom.

The features discussed above have been obtained using either so called $A=80$ parameters [10] or standard parameters [11]. The aim of the present study is to investigate if the difficulties can be overcome if different single-particle parameters are used. Especially, we generalize the modified oscillator potential so that we have full freedom when finding optimal positions for the subshells.

To aid us in our search, we used Hartree-Fock (HF) and relativistic mean field (RMF) calculations to investigate the variation of the position of the j-shells with mass. We found this mass-dependence to be quite strong and especially that these models suggest that the $f_{5/2}$ subshell comes below the $p_{3/2}$ in the upper half of the $Z,N=28-50$ shell. This is contrary to the ordering of these subshells in the parametrizations mentioned above which appear to be valid lower down in the $Z,N=28-50$ shell. Supported by these findings, we have tried to fit the position of the subshells in the modified oscillator model to reproduce the observed bands in ^{86}Nb, ^{87}Nb and ^{86}Zr as well as possible.

Since this is the first calculation for ^{86}Nb using the cranked Nilsson-Strutinsky model (CNS) we present a detailed discussion for this nucleus including total energies, Q_t-values and deformation paths. The results for ^{87}Nb and ^{86}Zr are only discussed briefly. In general, we get an improved understanding of the structure of the high-spin bands in these $A=86$, 87 nuclei. However, the new parameters are not without problems and in the summary we discuss some reasons why they might be expected.

II. MODEL

The calculations of the band structure and deformation paths in the $A=86$, 87 nuclei were performed using the configuration-dependent cranked Nilsson-Strutinsky model or for short the CNS-model [1,11]. In this model the deformed potential is rotating uniformly around a fixed axis and the rotation or rather the effects of the rotation is treated as an external potential.

A. Single-particle orbitals

The Hamiltonian used to describe a nucleon in the rotating nucleus is the cranked Nilsson (modified oscillator) Hamiltonian [11,12]

$$h^{\omega} = h_{\text{h.o.}}(\varepsilon_2,\gamma) - V' - \omega j_x + 2\hbar\omega_0\rho^2\varepsilon_4 V_4(\gamma), \qquad (1)$$

where $h_{\text{h.o.}}$ is an anisotropic harmonic oscillator whose deformation is defined by ε_2 and γ. The second term of the Hamiltonian is of the form

$$V' = \hbar\mathring{\omega}_0\kappa_N(N)\{2\mathbf{l}_t\cdot\mathbf{s} + \mu_N(N)(\mathbf{l}_t^2 - \langle\mathbf{l}_t^2\rangle_N)\}.$$

The index t in the orbital angular momentum operator $\mathbf{l}_t$ indicates that it is defined in stretched coordinates [13]. The $\mathbf{l}_t\cdot\mathbf{s}$ and $\mathbf{l}_t^2$ terms are usually made dependent on N by introducing an N-dependence for the two constants κ and μ.

When making the transition from the laboratory coordinate frame to the intrinsic (body-fixed) frame, the new term ωj_x appears, which expresses the centrifugal and Coriolis force existing in the rotating coordinate system. Furthermore one also includes a higher order hexadecapole deformation, $2\hbar\omega_0\rho^2\varepsilon_4 V_4(\gamma)$, where ρ is the radius in the stretched coordinate system.

The Hamiltonian is diagonalized using the eigenfunctions of the rotating oscillator [14], $|n_x n_2 n_3 \Sigma\rangle$, as basis states. The couplings between basis states of different $N_{rot}=n_x+n_2+n_3$ are small and therefore neglected. The main advantage of the rotating basis is thus that N_{rot} can be treated as an exact quantum number which is exploited when defining configurations as discussed below. The diagonalization of the Hamiltonian (1) gives the eigenvalues e_i^{ω}, which are referred to as the single-particle energies in the rotating frame or the *Routhians*.

B. The total energy of the nucleus

The total energy is obtained using the shell correction method. Thus, the shell energy, E_{sh}, is calculated using the Strutinsky procedure [15] and the total energy is then defined as the sum of the shell energy and the energy E_{rld}, obtained from the rotating liquid drop model [16],

$$E_{tot}(I) = E_{sh}(I) + E_{rld}(I). \tag{2}$$

This renormalization ensures that the total nuclear energy is correct on "the average." Finally, minimizing the total nuclear energy for a given angular momentum with respect to deformation gives the equilibrium shape and corresponding energy.

The transition quadrupole moments Q_t are calculated from the deformations assuming a uniform charge-density distribution ρ_0 inside the nucleus [1,17].

C. Configuration labeling in the CNS-model

A configuration in the CNS-model is a specification of which one-particle orbitals are occupied by nucleons. In order to follow how a specific configuration develops when the nucleus undergoes shape changes as it is being cranked up to higher and higher frequencies, one needs to keep track of the different orbitals. Following one orbital as the nucleus undergoes shape changes might seem like an easy task. However due to the strong mixing that occurs between the orbitals they exchange character and does not stay pure for long. One way to make it easier is to remove so-called "virtual crossings" [11]. A virtual crossing occurs when two orbitals come close to each other, exchange character and then separate again without actually crossing. To replace these virtual crossings with real crossings makes the orbitals develop more smoothly.

The parity- and signature-operators commute with the Hamiltonian. This makes it possible to associate every orbital with one parity and one signature. Furthermore, as mentioned above, the total oscillator shell quantum number $N_{rot} \equiv N$ is treated as pure which means that each orbital belongs to a specific N-shell.

A further tool is the classification into high- and low-j orbitals [18,19]. At spherical shape, the subshell with the highest value of j (the intruder shell) separates from the other j-shells within the N-shell and is found lower in energy. Although only approximate it is generally possible to make such a classification also for deformed shapes. Thus, in the present calculations the orbitals with the highest values of $\langle j^2\rangle$ in every N-shell have been classified as high-j orbitals.

The actual labeling of the nuclear configurations is done by specifying for each N-shell how many neutrons and how many protons that occupy orbitals of different signature α and high- and low-j character (see Sec. 3.6 of Ref. [1]). It is also convenient to define the quantity I_{max} as the maximum spin value which can be obtained in a specific configuration from rotation around the symmetry axis, i.e., from non-collective rotation with a specific distribution of the particles over the j-shells. Note that in principle any spin value can be obtained for collective rotation but values larger than I_{max} are generally of no experimental interest.

III. PARAMETERS

In order to get a good agreement with experiments one has to use parameters in the Nilsson potential that gives correct level ordering for the particular nucleus under consideration. Parameters approximately valid for large mass regions have been obtained by fitting to experimental data. For ^{86}Zr and ^{87}Nb previous calculations have been performed [5,8] using the $A=80$ parameters of Galeriu *et al.* [10] For ^{86}Zr these calculations reproduce the experimental bands to a large extent but there are reasons to believe that a better agreement could be achieved by modifying the parameters slightly. Similar conclusions can be drawn from an earlier study of ^{86}Zr using somewhat different parameters [9]. For ^{87}Nb, the calculations using $A=80$ parameters [5] appear not so good, when considering how well the model works in other regions [1]. For ^{86}Nb, no investigations using the CNS model have been published.

In order to investigate the level ordering and its variation with mass, Hartree-Fock (HF) and relativistic mean field (RMF) calculations were performed. The SIII parametrization [20] was chosen for the HF calculation since it has been widely used and is known to give a good description of a large variety of nuclear properties. For the RMF calculation the NL3 force was used [21]. HF calculations for all three nuclei using the same interaction revealed that the mass dependence among these three nuclei is very much negligible.

The mass dependence of κ and μ was discussed in Ref. [25], where evidence for a quite strong mass-dependence for μ was found. The main conclusion was that μ increases with mass within the $N=4$, 5 shells when going from one magic number to the next.

A similar trend for the $N=3$ shell can be seen in Fig. 1 where results from HF and RMF calculations are presented. In these calculations the number of neutrons was gradually increased from 20 to 50 and the number of protons was adjusted to keep the nucleus close to the line of β-stability. The $N=3$ shell starts getting filled when the number of neutrons exceeds 20 and when the number reaches 50 the $N=3$ shell

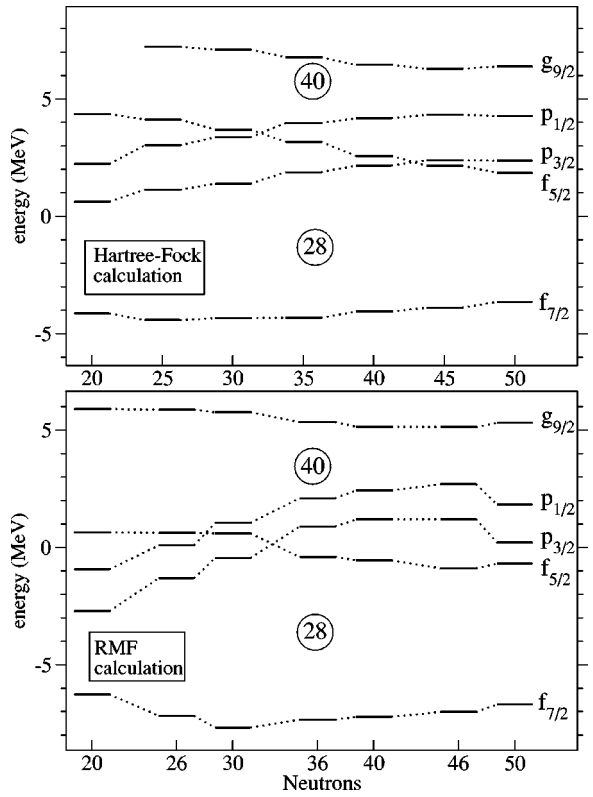

FIG. 1. Mass-dependence of the $N=3$ and $g_{9/2}$ single-neutron energies. The upper panel shows a spherical Hartree-Fock (HF) calculation using SkyrmeIII parameters and the lower panel a spherical relativistic mean field calculation using the NL3 force. The energies are plotted as a function of neutron number in the range $N=20-50$ along the β-stability line. The different energies are placed so that the mean values of the $N=3$ orbitals is constant, i.e., the absolute values on the y axis have no significance.

and the $g_{9/2}$ subshell are completely filled. Both the HF and the RMF calculations show the same trend with mass which can approximately be reproduced by increasing μ with increasing N in the $N=20$-50 range. For the nuclei investigated, the $p_{3/2}$ shell is below the $f_{5/2}$ shell for lower mass numbers but with increasing mass the ordering of these subshells is reversed. The three nuclei considered here have masses ~ 90 which means that it seems reasonable to use a larger μ than in the $A=80$ parameters. This larger μ-value has the effect of increasing the cost for the different configurations to build the last units of spin, since these maximal spin states are built with holes in the low-lying $f_{5/2}$ subshell.

A natural explanation for the mass trend comes from the filling order of the orbitals. When the $f_{7/2}$ subshell is filled the density is moved away from the center of the nucleus. This creates a deeper potential at some distance away from the center and the $N=3$ particles which can take most advantage of this deeper potential are the ones in the $f_{7/2}$ and $f_{5/2}$ subshells. As the $f_{5/2}$ subshell starts being filled, the $l=3$ nucleons benefit even more and the overall effect can be described by an increasing μ.

From a shell model point of view, it has been discussed how the monopole interaction between spin-orbit partners like $d_{5/2}$ and $d_{3/2}$ in the sd-shell or $g_{9/2}$ and $g_{7/2}$ in the $A=100$ region leads to an effective lowering of these subshells [22,23]. Even though parts of this effect would probably be described as caused by deformation in a mean field approach, it is interesting to note how the analogous interaction between the $f_{7/2}$ and $f_{5/2}$ partners should lead to a lowering of the $f_{5/2}$ subshell when particles are added to the $f_{7/2}$ subshell (cf. Fig. 1). It is also interesting to note that the neutron-proton interaction gives the main contribution, see also Ref. [24].

Potential altering effects could also occur with many particles excited to $g_{9/2}$. In this case excited configurations are formed by emptying $p_{3/2}$ and $p_{1/2}$ orbitals and filling $g_{9/2}$ orbitals which leads to a decrease in density close to the center of the nucleus and an increase further away, favoring the high-j shells.

The shallower potential closer to the center might affect the spin-orbit potential which is generally taken to be proportional to the derivative of the central potential. It was shown in [26] that for j-states with large occupation probabilities in a region of reduced density, the amplitude of the spin-orbit splitting is sometimes greatly reduced. Such configuration dependent effects, which are assumed to be small, might be simulated in the present model with some configuration dependence of the parameters. However no such attempts are made here.

In Fig. 2, four sets of energy levels corresponding to different parameters are shown. The spherical single-particle energies corresponding to standard parameters [11] and to $A=80$ parameters [10] are shown together with the energies obtained from fits to the high-spin bands in ^{86}Nb and ^{87}Nb (set A) and in ^{86}Zr (set B), respectively. These fits are certainly not unique but as discussed below, they clearly lead to an improved agreement between the observed bands and the calculated configurations. Note especially that, in agreement with the HF and RMF calculations, the fits predict a lowering of the $f_{5/2}$ subshell for these nuclei with only a few holes in the $N=3$ shell.

In order to obtain more freedom when finding parameters for this region we introduced an l-dependence for κ and μ in addition to the N dependence. This gives us full freedom when placing the j-shells. However we keep one restriction, namely that the mean value of every N-shell is preserved. The new freedom can be utilized for example to place the j-shells as predicted by a Woods-Saxon potential as in Ref. [27]. The spherical Nilsson energies $e_{N,l,j}$ corresponding to the parameters used are listed in Tables I and II.

The parameters describing the surface and Coulomb energies in the rotating liquid drop energy, Eq. (2), are taken from Ref. [28]. The corresponding rigid body moment of inertia is calculated assuming a uniform mass distribution inside a volume of $(4/3)\pi r_0^3 A$ with $r_0=1.2$ fm.

IV. CALCULATED ROTATIONAL BAND STRUCTURES IN ^{86}Nb

In the calculated potential energy surfaces for $I\simeq 10-30$, minima are generally seen at $\epsilon_2=0.15-0.25$, $\gamma=-40--60$. In single-particle diagrams calculated for these deformations, there is a gap at 43 particles for both protons and neutrons

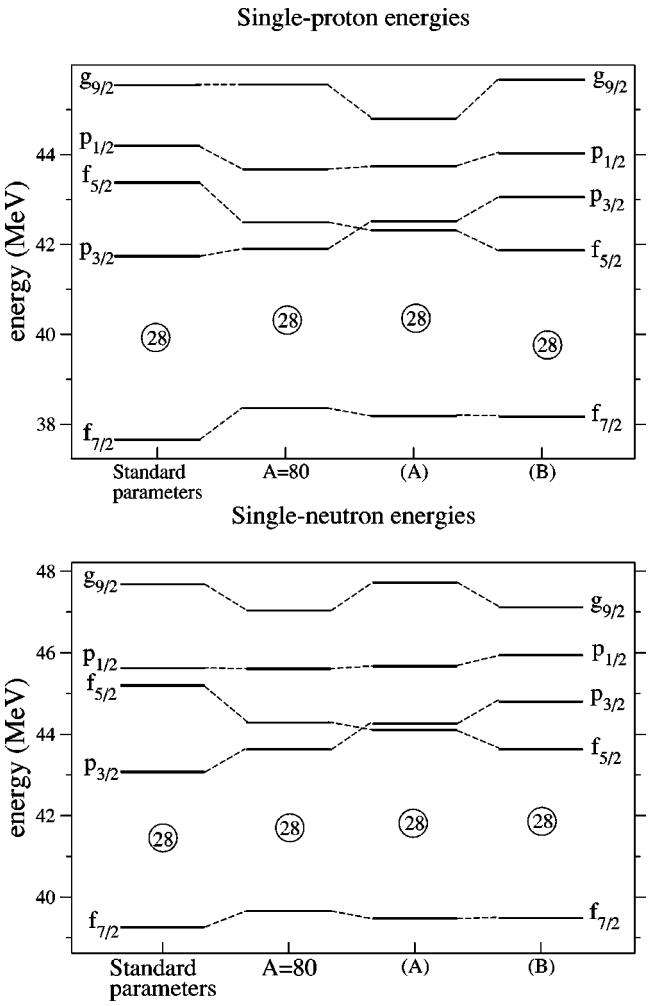

FIG. 2. Spherical single-proton (upper panel) and single-neutron energies (lower panel) calculated with a modified oscillator potential for different choices of parameters. Sets A and B were found by fitting to experimental excitation energies in ^{86,87}Nb and ^{86}Zr, respectively. Both sets A and B produce the same ordering between the $f_{5/2}$ and $p_{3/2}$ subshells as predicted by the HF and RMF calculations.

corresponding to 5 $g_{9/2}$ particles and two $N=3$ holes. As seen in Fig. 3 the most favored proton configurations are formed with two holes below this gap, i.e., with 3, 4 or 5 $g_{9/2}$ protons and the most favored neutron configurations contain two particles above the gap i.e., 5, 6 or 7 $g_{9/2}$ neutrons.

In this mass region, configurations are often labeled by the number of $g_{9/2}$ particles, see Ref. [1]. Here, we will use a more complete labeling, namely two digits and a + or − sign so that also the signature within the different groups of orbitals is specified. The first digit shows the number of holes in the $N=3$ orbitals and the second digit the number of

TABLE I. Spherical Nilsson energies in units of $\hbar\omega_0$ resulting from parameter set A.

$e_{N,l,j}$	Protons	Neutrons
$e_{4,4,9/2}$	4.943	5.068
$e_{3,3,7/2}$	4.207	4.186
$e_{3,3,5/2}$	4.662	4.676
$e_{3,3,3/2}$	4.684	4.693
$e_{3,3,1/2}$	4.819	4.843

TABLE II. Spherical Nilsson energies in units of $\hbar\omega_0$ resulting from parameter set B.

$e_{N,l,j}$	Protons	Neutrons
$e_{4,4,9/2}$	5.028	4.996
$e_{3,3,7/2}$	4.208	4.187
$e_{3,3,5/2}$	4.612	4.626
$e_{3,3,3/2}$	4.742	4.751
$e_{3,3,1/2}$	4.847	4.871

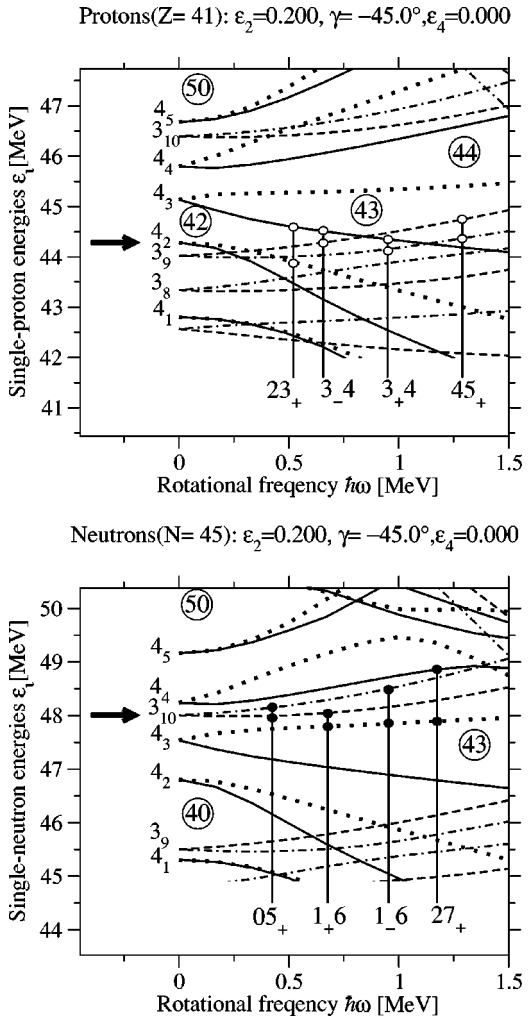

FIG. 3. Single-proton (upper panel) and single-neutron (lower panel) energies at a typical deformation of ^{86}Nb shown as a function of cranking frequency ω. The energies are calculated using parameter set A. At this deformation, the relevant proton configurations are built by creating two holes below the $Z=43$ gap, indicated by open circles, and the important $N=45$ configurations are formed by placing two neutrons, indicated by closed circles above the $N=43$ gap. The configurations are labeled by the number of $N=3$ holes and $g_{9/2}$ particles as explained in the text.

Neutron configurations

Proton configurations	12.5^+ 05_+	11.5^+ 05_-	14.5^- 1_+6	13.5^- 1_-6	14.5^+ 27_+	13.5^+ 27_-
23_+	(+,1)	(+,0)	(−,1)	(−,0)	(+,1)	
14.5^+	27^+	26^+	29^-	28^-	29^+	
23_-			(−,0)		(+,0)	
13.5^+			28^-		28^+	
3_+4	(−,1)		(+,1)		(−,1)	
16.5^-	29^-		31^+		31^-	
3_-4	(−,1)		(+,0)		(−,0)	
17.5^-	30^-		32^+		32^-	
45_+			(−,1)	(−,0)	(+,1)	(+,0)
18.5^+			33^-	32^-	33^+	32^+
45_-						
17.5^+						

FIG. 4. Combination of the more interesting $Z=41$ proton and $N=45$ neutron configurations to total configurations for ^{86}Nb. The proton and neutron configurations are labeled by the number of $N=3$ holes and $g_{9/2}$ particles and by the signature for an odd number of particles as explained in the text. The maximum spin values I_{max}, calculated under the assumption that a distinction can be made between orbitals of $f_{7/2}$ character and the other $N=3$ orbitals, are also given. Parity and signature (π,α) of the configuration is indicated along with the spin I_{max} of the total configuration. Positive parity configurations are shown on a shaded background. The favored configurations in each group containing the same number of $g_{9/2}$ particles are underlined. Configuration $[1_+2,05_+]$ is not included since it has a different deformation as seen in Fig. 12 below.

particles in the $g_{9/2}$ subshell. The sign is given as a subscript of an odd number of particles and indicates the signature α of those particles. No subscript is given for the standard case of $\alpha=0$ for a even number of particles while two + signs are shown for the specific case with two more particles in $\alpha=1/2$ than in $\alpha=-1/2$.

The most important total configurations are illustrated in Fig. 4. They are built from the configurations indicated in Fig. 3 and in addition signature partners so that in total six proton and six neutron configurations are included. The energy of the low-lying total configurations is now calculated and the minima are followed through deformation space $(\epsilon_2,\epsilon_4,\gamma)$ as they are cranked to higher spins. These minimized energies of ^{86}Nb are shown relative to a rigid rotor reference in Fig. 5. The main reason for subtracting the "standard" [29] rigid rotor reference $[E_{rld}=(\hbar^2/2J_{rig}I(I+1)$ with $\hbar^2/2J_{rig}=0.007(158/A)^{5/3}$ MeV=18.9 keV] is to remove the dominant quadratic dependence on spin making it possible to show the energy difference on an expanded scale. Furthermore, by using the same (A-dependent) reference for all nuclei, it becomes possible to compare the generation of angular momentum in different mass regions, see e.g., Ref. [1]. In this approach, pairing correlations are neglected which means that calculations are realistic only for states with spins above $\approx 15\hbar$, i.e., it is only for these spin values we can expect any quantitative agreement between calculations and experiment.

One important fact when comparing calculations and experiment in ^{86}Nb is that one band, namely band 6, has been observed to the very high spin $I^\pi=33^-$. Considering the configurations shown in Fig. 4, the only theoretical counterpart is achieved with 5 $g_{9/2}$ protons and 6 $g_{9/2}$ neutrons. Another configuration terminating at $I=33^-$ is obtained with 6 $g_{9/2}$ protons and 7 $g_{9/2}$ neutrons, but particles are excited across the 43 gaps in this configuration which makes it much higher in energy. Core excited configurations are also calculated much higher in energy and thus less interesting for the spins observed.

The $[45_+,1_+6]$ configuration which will thus be identified with band 6 is drawn in the lower right panel of Fig. 5. It is necessary that this band with relatively many $g_{9/2}$ particles comes in the yrast region which requires that the $g_{9/2}$ subshell for protons must be relatively low in energy. This was one important constraint when fixing parameter set A. Indeed, with the $A=80$ parameters, this configuration comes too high in energy to make it a reasonable candidate for band 6. A similar difficulty was noticed for ^{87}Nb in Ref. [5] where, using $A=80$ parameters, no theoretical counterpart with $I_{max}=61/2$ was found for band 3 observed to $I^\pi=(61/2)^-$ and where it is only for configurations with 5 $g_{9/2}$ protons that such a high spin value can be achieved.

Another important feature of the bands drawn in Fig. 5 is that most bands show a relatively smooth behavior with a tendency to slope more and more upwards close to $I=I_{max}$ when the number of $g_{9/2}$ particles increases. This is contrary to the bands obtained with $A=80$ parameters where the bands have a stronger downward slope at high spin which is also seen in the calculation for ^{87}Nb [5]. This difference is mainly due to the relative positions of the $p_{3/2}$ and $f_{5/2}$ subshells, where the lower $f_{5/2}$ position with present parameters leads to a higher energy to build the highest states in general agreement with experiment. To conclude this subsection, it is important to realize the difficulties to make an objective fit of the single-particle parameters, i.e., the parameter sets used here are certainly associated with some arbitrariness.

A. Positive-parity structures in ^{86}Nb and comparison with experiments

The observed positive-parity bands of ^{86}Nb [7] are drawn in the upper panel of Fig. 6. It is especially bands 2 and 3 which are low in energy at high spin and where one could hope to find calculated counterparts. Comparing with Fig. 5, the $\alpha=1$ configurations $[23_+,05_+]$ and $[45_+,27_+]$ appear to describe these bands quite well. They are thus drawn in the lower panel of Fig. 6 together with the signature partner $[45_+,27_-]$ which could then be expected to describe band 4. Additionally, the signature partners $[23_\pm,27_+]$ which might be an alternative interpretation of bands 3 and 4 are drawn in the lower panel of Fig. 6. Finally, also the closed core configurations $[01_+,05_\pm]$ are drawn in Fig. 6. The closed core configurations terminate at $I^\pi=16^+,17^+$ at oblate shape, $\gamma=60^\circ$. Their deformations are thus very different from that of

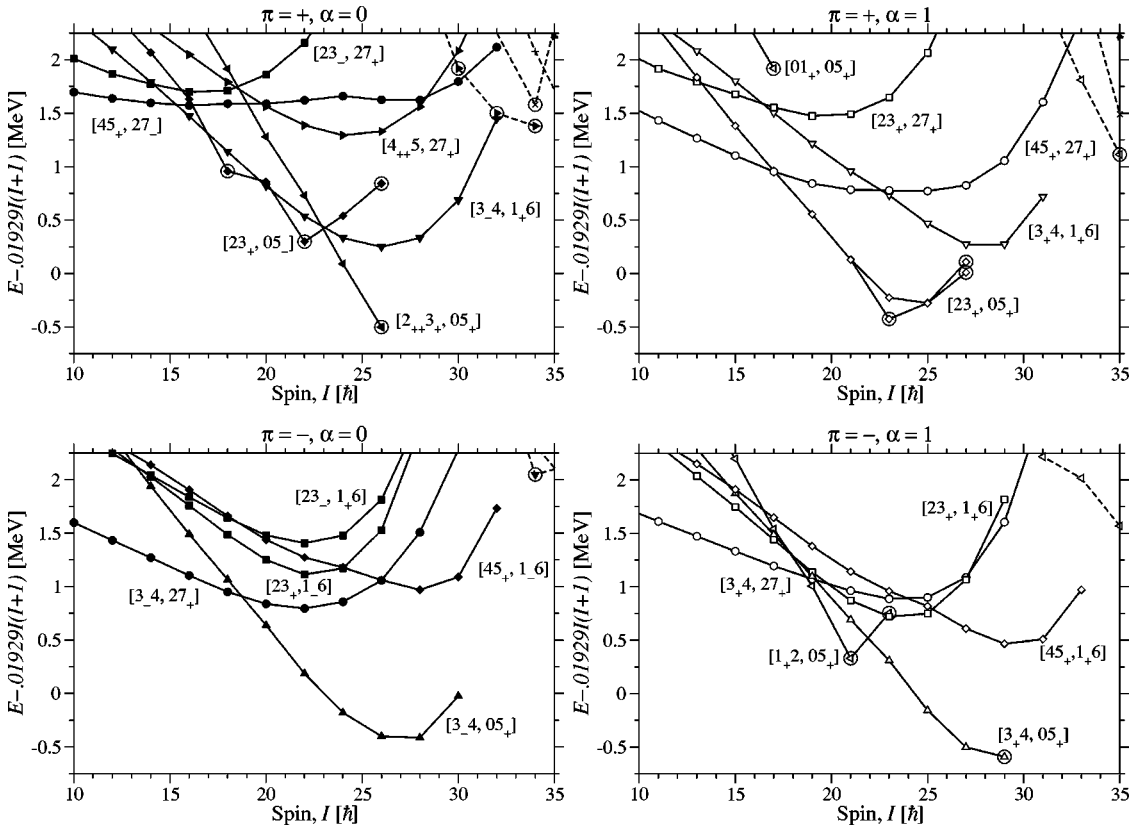

FIG. 5. Calculated total energies of ^{86}Nb relative to a rigid rotor reference. Parameter set A, which has been fitted to optimize the agreement between experiment and theory, is used in the CNS calculation. Terminating states are indicated by large open circles. Dashed lines are used for configurations built from particle-hole excitations across the 50 gap. These core-excited configurations are considerably higher in energy than the valence space configurations and thus less likely to be associated with experiment.

the more collective configurations illustrated in Fig. 4 which is the reason why they are not included in that figure. It seems however that they could be the theoretical counterpart of the observed $16^+, 17^+$ states at 5027 and 5533 keV, [7] which are drawn in the upper panel of Fig. 6 and which appear to have a somewhat reduced collectivity.

Let us now discuss the more interesting bands in some detail, i.e., bands 2, 3 and 4.

1. Band 2

The two states drawn for $I=23$ in the lower panel of Fig. 6 correspond to different minima in the potential energy surface shown in Fig. 7. The configuration has five neutrons in $g_{9/2}$ coupling to a maximum spin of $12.5\hbar$. The three protons in $g_{9/2}$ couple to a maximum spin of $10.5\hbar$ which makes a total of $23\hbar$. One possibility is then to couple the proton holes to spin zero. This can be done by putting them both in $p_{1/2}$ which creates the minimum at $\gamma=60$ in the $I=23$ potential energy surface shown. At $\gamma=60$ the symmetry axis is the cranking axis implying that this 23^+ state is aligned and thus encircled in Fig. 6.

The other minimum in Fig. 7 can be followed in deformation and reaches $\gamma=60$ at $I=27\hbar$. At this spin, two states are marked. The lowest energy state is obtained by putting the proton-holes in orbitals of $f_{5/2}$ and $p_{3/2}$ character, respectively, and the excited state comes from putting them both in $f_{5/2}$, as can be understood from Fig. 2 above. In both cases, these two holes couple to $I=4$ combined with $I=23$ from the $g_{9/2}$ particles.

Examining the Q_t values shown in Fig. 8, there seems to be no strong indication of band termination although the Q_t values for band 2 decline somewhat toward the maximum spin seen. Note however that the last values are pretty uncertain. Overall the calculated Q_t values for the $[23_+, 05_+]$ configuration are in good agreement with experiment. The Q_t-value in connection with the $I=23$ state is calculated using the higher energy collective minimum which appears consistent with experiment.

2. Bands 3,4

These bands are connected through a sequence of M1 transitions which exhibit an alternating pattern in the B(M1) strengths. This is not surprising considering, e.g., Ref. [30] where it was found that even a small rotation has a drastic effect on the transition matrix elements between nucleons in high-j orbitals. Basically the result predicts that M1-transitions from the unfavored to the favored band are in some cases much suppressed compared to transitions from the favored to the unfavored band which probably explains the observed B(M1) values. As concluded above, the configurations most likely to be associated with these bands are the signature partners $[45_+, 27_+]$ and $[45_+, 27_-]$. Examining

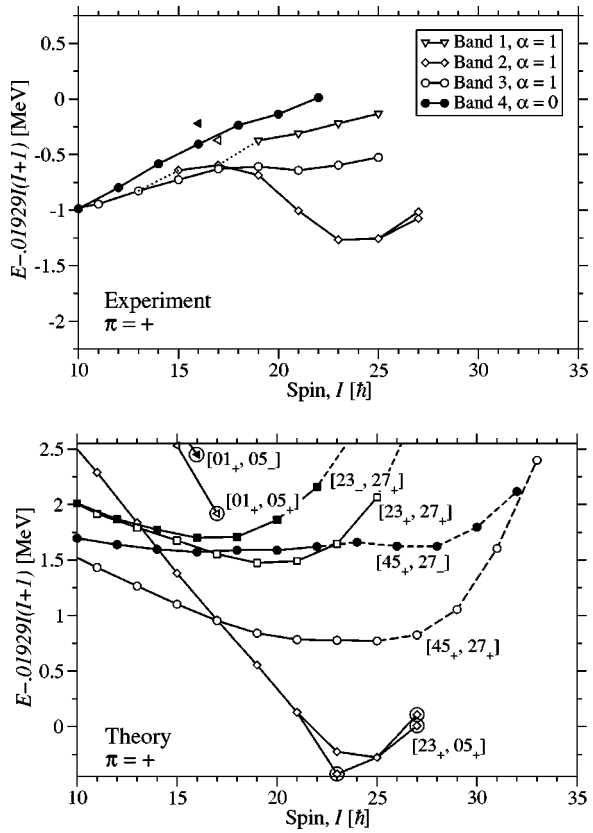

FIG. 6. Comparison between experimental (upper panel) and calculated (lower panel) energies in ^{86}Nb relative to a rigid rotor reference. Only configurations with positive parity likely to be identified with experiment are displayed. Also shown are the 16^+ and 17^+ states which are naturally interpreted as the closed core [01,05] configurations. Closed symbols are used for signature $\alpha=0$ and open symbols for $\alpha=1$. Dotted lines indicate some of the transitions between the experimental bands. Identical symbols are used in the two panels to indicate our preferred interpretation. Dashed lines in the lower panel indicate those parts of the calculated bands not seen in experiments, according to present interpretation.

the Q_t values shown in Fig. 8 the agreement is less satisfying. Both configurations seem to be too deformed and thus too collective to be good candidates. There are two other signature partners with Q_t values in better agreement with experiments. These are $[23_-,27_+]$ and $[23_+,27_+]$ which are less deformed and thus with Q_t values closer to the experiment. However Fig. 6 shows that these configurations are located somewhat too high in energy, especially at the highest observed spin values, to be really good candidates for bands 3 and 4.

3. Deformation trajectories

The deformation paths for some of the more interesting configurations are depicted in Fig. 9. Note that these configurations tend to be oblate which is understood from the fact that they are most naturally described as hole states, especially the [45,27] configurations for which both the $g_{9/2}$ subshell and the $N=3$ low-j shells are more than half full. It is also interesting to note that these configurations do not reach

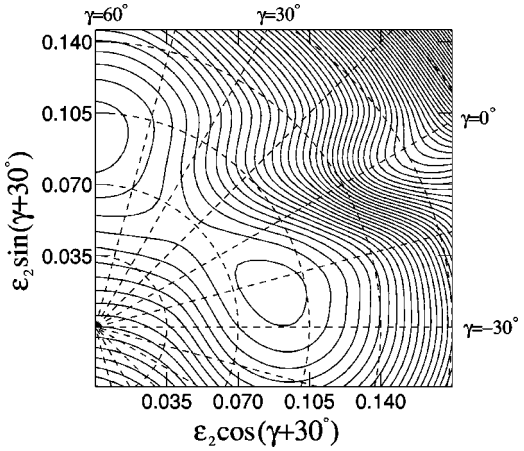

FIG. 7. Potential energy surface for the positive-parity configuration $[23_+,05_+]$ at $I=23\hbar$. Each lattice point has been minimized with respect to ε_4-deformation. The contour line spacing is 0.1 MeV.

the non-collective $\gamma=(-120°,60°)$ axis at their I_{max} values.

The $[23_+,05_+]$ has fewer particles excited to $g_{9/2}$ which leads to a different deformation than the other configurations. There is a forking at $I^\pi=23^+$ in the deformation path of this configuration which is caused by the second minimum in Fig. 7. This means that the nucleus in this case has two paths to choose from and choosing the smoothest path increases the energy for the $I^\pi=23^+$ state.

B. Negative-parity structures in ^{86}Nb and comparison with experiment

The observed negative-parity bands are drawn in the upper panel of Fig. 10. Bands 5 and 6 are regular bands in the $I\approx 20-30$ range while band 9 is low-lying up to the highest spin value observed, $I=23$; i.e., it is mainly for these three bands that we could hope to find theoretical counterparts. Comparing with the calculated bands in Fig. 5, the

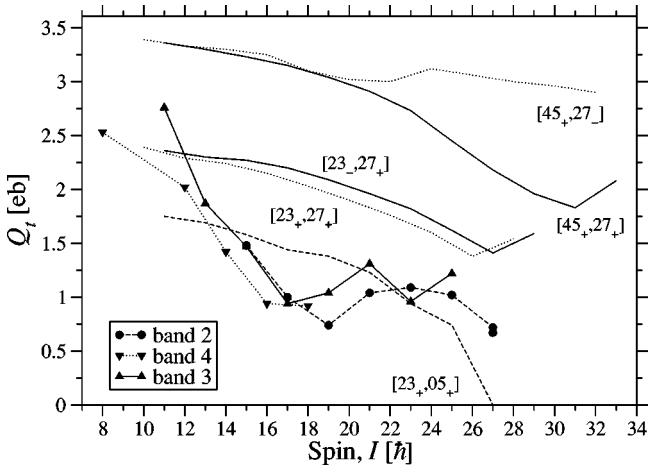

FIG. 8. The electric transition quadrupole moments Q_t vs initial spin I_i for the positive parity bands. Experimental values for bands 2, 3, and 4 are compared with the calculated values for some configurations.

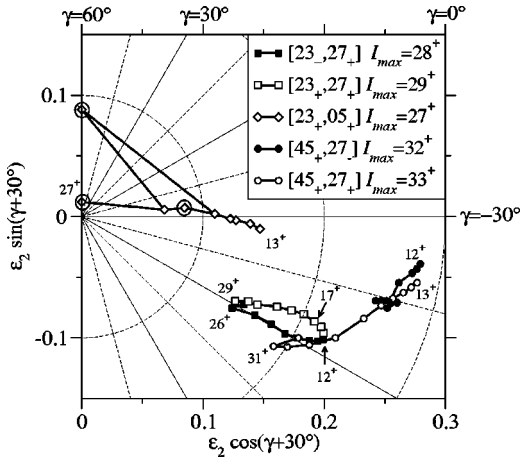

FIG. 9. Calculated deformation trajectories for the configurations considered in Fig. 6. For the trajectories drawn, the deformation decreases with increasing spin. The trajectories are drawn in steps of $\Delta I=2$ up to $I=I_{max}$.

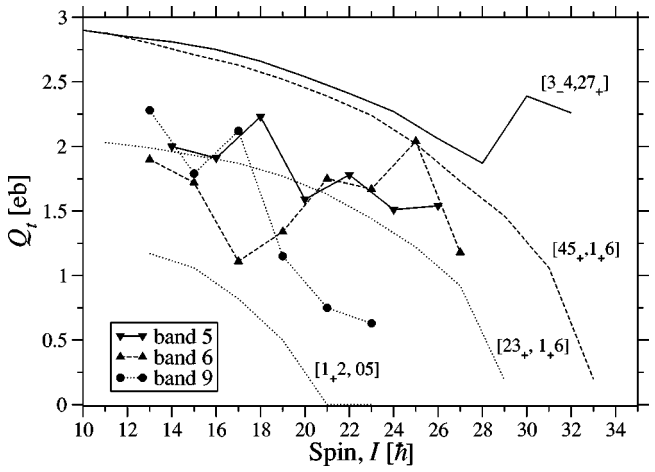

FIG. 11. The electric transition quadrupole moments Q_t vs initial spin I_i for the negative parity bands in ^{86}Nb. Experimental values for bands 5, 6 and 9 are compared with the calculated values for some configurations.

$[3_-4,27_+]$, $[45_+,1_+6]$ and $[1_+2,0.5_+]$ configurations appear to describe the high spin energy characteristics of these observed bands quite well. They are thus drawn in the lower panel of Fig. 10 together with two more bands, namely $[3_+4,27_+]$ and $[23_+,1_+6]$. The former configuration should probably be identified with the lower spin range of band 6, where connecting M1 transitions indicate that it is the signature partner of band 5, while the latter configuration is an alternative interpretation of band 9.

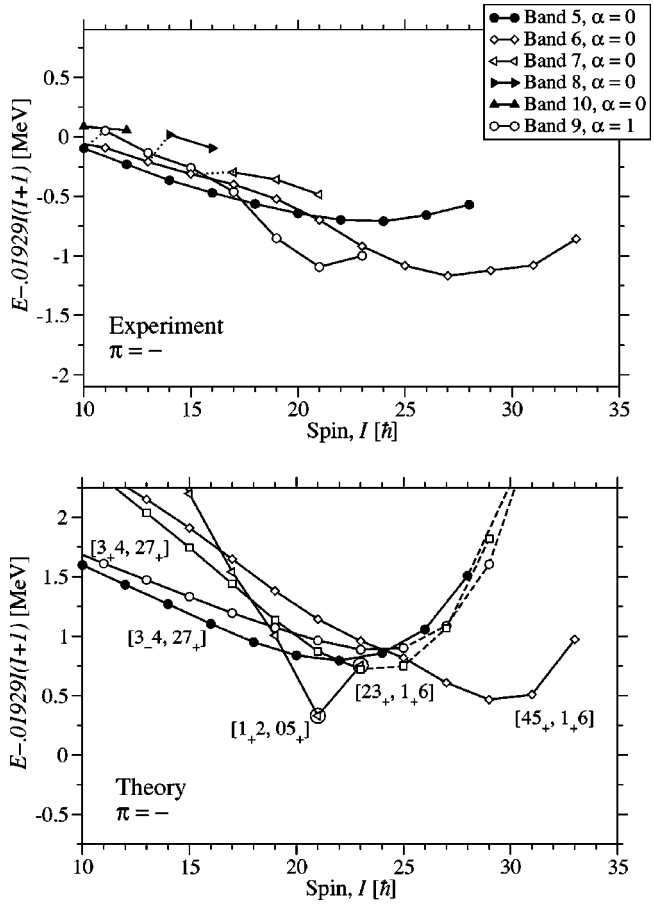

FIG. 10. Comparison between the experimental (upper panel) and calculated (lower panel) energies of negative parity in ^{86}Nb relative to a rigid rotor reference. The different rotational bands are drawn in a similar way as the positive parity bands in Fig. 6.

1. Bands 5 and 6

As mentioned above, because band 6 proceeds to spin 33 $\hbar$, it can only be associated with the $[45_+,1_+6]$ configuration having $I_{max}=33$, see Fig. 5. Furthermore the assignment of band 5 to the $[3_-4,27_+]$ configuration is very solid in the sense that this interpretation is essentially independent of parameters. These assignments can also be tested by comparing observed and calculated Q_t values as shown in Fig. 11. The observed values for bands 5 and 6 show large fluctuations, probably because of band mixing. Therefore, we cannot expect the calculated values for pure configurations to come very close, and the fact that the observed values are generally somewhat lower than the values calculated for configurations $[3_-4,27_+]$ and $[45_+,1_+6]$ is not unexpected. Note also that the Q_t values have not been determined at high enough spin to give much clues about band termination. The deformation paths for these configurations are shown in Fig. 12. As in the positive-parity case, the configurations are predicted to have deformations around $\gamma=-40°--60°$, i.e., Fig. 3 can be consulted to get a better understanding of the relevant single-particle orbitals. Note also that these bands do not reach the non-collective axis even at their I_{max} values. Comparing Figs. 11 and 12, the discontinuity in the Q_t versus spin curve for configuration $[3_-4,27_+]$ can be understood from the corresponding shape trajectory where a jump in deformation is calculated. The jump is due to a rather large and shallow energy minima in the total energy surface for spin values $I=28-32$. In this case, choosing a more continuous path similar to that for the signature partner $[3_+4,27_+]$ results in only a small energy cost and might be considered the more physical path since it results in a more continuous variation of the wave function.

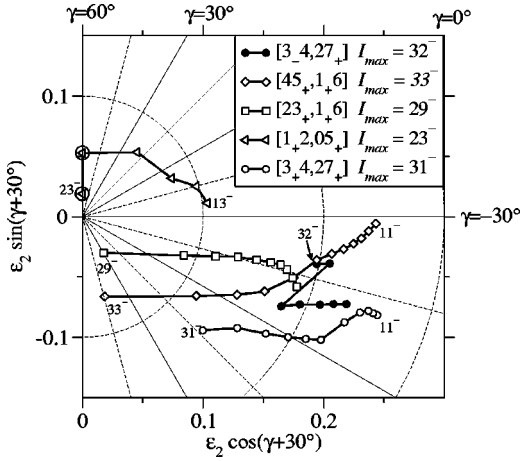

FIG. 12. Same as Fig. 9 but for negative parity configurations of ^{86}Nb.

2. Band 9

The most natural candidate for band 9 is certainly the configuration $[1_+2,05_+]$. The calculated band comes down somewhat too steep in Fig. 10, but it is at the right position and its I_{max} value corresponds to the highest spin state observed in band 9 indicating that it terminates at this spin value. Another assignment could be configuration $[23_+,1_+6]$ which is at the right place and not as steep but does not terminate until spin $29\hbar$. For this band, the experimental Q_t-values are located between those calculated for the two configurations, see Fig. 11. The decline among the last three observed Q_t values and the sharp bend in the energy versus spin curve at the last spin seem to support the band termination interpretation based on the $[1_+2,05_+]$ configuration. Similar conclusions can also be drawn from the observed γ-ray intensities [31] which show a large decrease when approaching the $I=23$ state.

C. Discussion of ^{86}Nb configurations and comparisons with ^{87}Nb

With the assignments above, we have found calculated configurations of ^{86}Nb which describe the energy characteristics of all low-lying high-spin bands, 2,3,5,6 and 9 quite well. There are however two configurations displayed in Fig. 5 that are calculated low in energy but with no experimental counterpart, namely the signature partners $[3_-4,05_+]$ and $[3_+4,05_+]$. Considering Fig. 4, the observed bands are assigned to configurations in the upper left as well as in the lower right corner, i.e., configurations with large difference in the total number of $g_{9/2}$ particles. Therefore, the problem with the low [34,05] configurations, with an intermediate number of $g_{9/2}$ particles, cannot be cured by a variation in the same direction of the proton and neutron $g_{9/2}$ subshells. If the $g_{9/2}$ subshells were lowered it corresponds to a favoring of configurations with many $g_{9/2}$ particles so that the [34,05] bands would come even lower relative to the [12,05] and [23,05] configurations assigned to bands 2 and 9. If the energy of the $g_{9/2}$ subshells were increased on the other hand, it leads to similar problems for the [34,05] configurations relative to the configurations with more $g_{9/2}$ particles assigned to bands 3, 5 and 6. Such changes will thus only destroy the balance between configurations with few and many $g_{9/2}$ particles but not help to increase the relative energy of the [34,05] band which have no experimental counterpart. On the other hand, we may note that the unobserved [34,05] bands have relatively many $g_{9/2}$ protons being located to the left in Fig. 4. Therefore, if the $g_{9/2}$ proton subshell was lifted relative to that for neutron, it would in general increase the energy of these "unobserved configurations" relative to those assigned to experimental bands. This puts some doubt on present parameter set A in Fig. 2, with the proton $g_{9/2}$ subshell considerably lower than that for neutrons. These positions are however required to get the relative energies of the configurations assigned to band 5 and 6 in agreement with experiment, especially the low energy for the configuration $[45_+,1_+6]$ with $I^{\pi}_{\max}=33^-$, which is assigned to band 6.

Another configuration which appears low in Fig. 5 is $[2_{++}3,05_+]$. However it is coming down very steep and is low in energy only for $I=24^+$ and 26^+. Furthermore it has a somewhat strange feature with the same signature for both $N=3$ holes. Therefore, it is not surprising that it does not have any experimental counterpart.

As mentioned above, the parameters used for ^{86}Nb have been fitted to the level scheme of both ^{86}Nb and ^{87}Nb. Indeed, the level scheme in these two nuclei have large similarities with most band in ^{86}Nb having their counterparts in ^{87}Nb. The detailed results for ^{87}Nb can be found in Ref. [5] and will not be presented here. In general however, with the new parameters, the bands are less down-sloping close to termination when drawn versus the standard reference in general agreement with experiment. There are however similar problems as in ^{86}Nb, e.g., with calculated low-lying bands with 4 $g_{9/2}$ protons and 6 $g_{9/2}$ neutrons which have no experimental counterpart. The fact that the low-lying calculated [34,05] bands have no correspondence in the presently observed level scheme of ^{86}Nb (and the [34,06] bands in the level scheme of ^{87}Nb) suggest some adjustment for the relative energies of the calculated bands. In any case, however, these configurations are expected to come relatively low in energy making it worthwhile to continue the search for the corresponding bands in the experimental level scheme.

V. HIGH-SPIN BANDS IN ^{86}Zr

The level scheme of ^{86}Zr has been analyzed using both standard parameters [8] and another parameter set similar to $A=80$ parameters [9]. In general the assignments of the high-spin bands seem pretty clear. Therefore this nucleus constitutes a useful playground when investigating different parameters in this mass region.

In Fig. 13 all observed positive-parity bands have signature $\alpha=0$ corresponding to even spin values. In the middle panel of Fig. 13 the parameters labeled (A) have been used which are the ones fitted to ^{86}Nb and ^{87}Nb. The configurations likely to be identified with experiments are [44,06] and [22,06]. Note that the relative positions of these two high-spin bands are not well reproduced with these parameters. In the lower panel, single-particle parameters fitted to ^{86}Zr (set

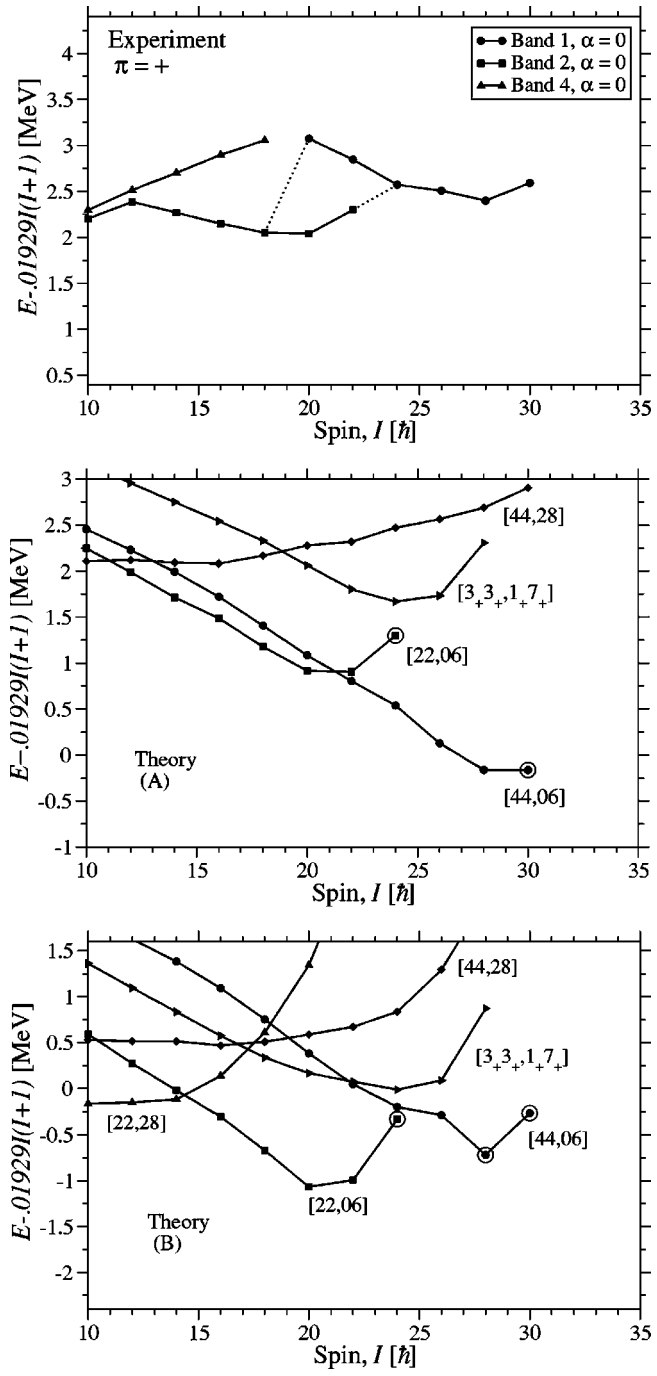

FIG. 13. Comparison between the experimental (upper panel) and calculated (lower panels) energies in ^{86}Zr relative to a rigid rotor reference. Only bands with positive parity are drawn. Case (A) is calculated with the same parameters as for ^{86}Nb and case (B) is calculated with parameters more adapted to ^{86}Zr.

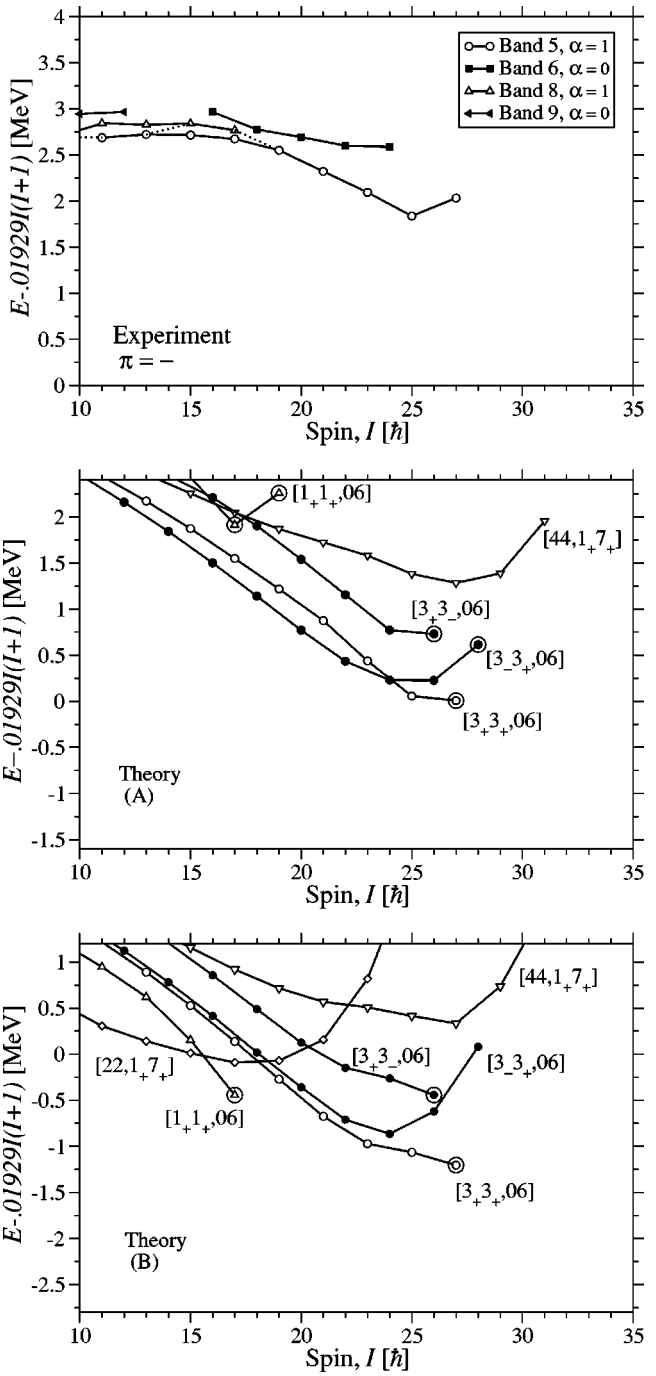

FIG. 14. Same as in Fig. 13 but for bands with negative parity.

B of Fig. 2 and Table II) have been used and the result looks more promising. Compared with the $A=80$ parameters the curves generally obtain more unfavored terminations for both parameter sets, A and B. This is caused by the lowering of the $f_{5/2}$ subshell and agrees better with experiment. Indeed, the agreement between experiment and calculation is quite good for parameter set B. Even the calculated aligned 28^+ state, built with the four $N=3$ proton holes coupled to $I=4$, appears supported by a discontinuity in the observed band. Then, for the $I=30^+$ state, the $N=3$ holes couple to their maximum spin, $I=6$.

In the negative-parity case (see Fig. 14), the two configurations likely to be associated with experiments are the signature partners $[3_+3_+,06]$ and $[3_+3_-,06]$. Both configurations are predicted rather low for both parameter sets and seems to be in fair agreement with experiments. Note that the even spin band is interpreted as a signature partner in the $g_{9/2}$ protons. Such high-j partners seem more likely to exhibit M1-transitions than those which have exchanged the signa-

ture of a nucleon in low-j orbitals. This is seen here and also seems to be the case for the negative parity bands in ^{87}Nb (Ref. [6]). For the favored negative parity band, the agreement has been pretty bad close to termination in previous calculations [8,9] and the more soft termination with present parameters comes much closer to experiment.

VI. CONCLUSIONS

In this study, we have tried to find improved single-particle parameters to describe the high-spin bands in ^{86}Nb and neighboring nuclei. The relative positions of the $N=3$ and $g_{9/2}$ subshells as functions of particle number have been investigated in self-consistent models. Furthermore, in configuration-dependent cranked Nilsson-Strutinsky calculations with the modified oscillator potential, the single-particle parameters have been varied to fit the observed bands. The most important conclusion, common to both studies is that contrary to the level ordering used in previous calculations, the $f_{5/2}$ subshell must be placed below the $p_{3/2}$ subshell in this mass region.

With the revised parameters, the general features of the rotational bands close to termination is described much better than before, i.e., when plotted relative to a standard rigid rotation reference, the calculated and observed bands have similar slopes as functions of angular momentum. Furthermore, it was possible to find reasonable interpretations of all low-lying high-spin bands of ^{86}Nb in terms of configurations with 7 to 12 $g_{9/2}$ particles. Indeed, states which most likely correspond to the maximum spin states in the closed core configuration with 6 $g_{9/2}$ particles $I=16^+,17^+$ were also identified. One problem is that one configuration with 8 $g_{9/2}$ particles is calculated as yrast for spin values $I\approx 20-30$ but it does not have any experimental counterpart. However, with uncertainties of 0.5–1.0 MeV in the relative positions of the different bands, such discrepancies are not too surprising. It was also suggested that in this region with a large variation in the number of high-j particles between different bands, the assumption that all bands can be described with the same single-particle parameters could be a somewhat rough approximation. It would thus be interesting to investigate if a better description could be achieved in self-consistent calculations.

Similar calculations were also tried for ^{86}Zr where, according to previous studies, the configurations of the different bands are well established. These calculations resulted in a good agreement between the lowest calculated bands and the observed high-spin bands. We also made some comments about the high-spin bands of ^{87}Nb which are very much analogous to those in ^{86}Nb and where one can also note similar successes and problems in the theoretical description.

In general, the high-spin bands in ^{86,87}Nb appear strongly mixed which is certainly a difficulty when comparing with the theoretical calculations, where pure configurations are assumed. This mixture will also make it difficult to observe the B(E2) transition probabilities for the pure bands. It is therefore not too disturbing that calculated B(E2)'s are in general somewhat bigger than the observed ones. One should also note that most of the bands are calculated as oblate or close to oblate. This is an interesting feature but somewhat unusual and could therefore lead to difficulties in the theoretical description. Another interesting fact is that it is only bands with few $g_{9/2}$ particles which are calculated to terminate and become non-collective when they reach I_{max}, i.e., most bands can be followed beyond the maximum spin state as calculated from their distribution of particles over the subshells. These states with $I>I_{max}$ are however quite high in energy and therefore it is very questionable if they could ever be identified in experiment.

ACKNOWLEDGMENTS

We would like to thank A. V. Afanasjev, who conducted the RMF calculation. This project was supported by the Swedish Science Research Council.

[1] A.V. Afanasjev, D.B. Fossan, G.J. Lane, and I. Ragnarsson, Phys. Rep. **322**, 1 (1999).
[2] I. Ragnarsson, Nucl. Phys. **A557**, 167c (1993).
[3] A.V. Afanasjev and I. Ragnarsson, Nucl. Phys. **A608**, 176 (1996).
[4] C.E. Svensson, C. Baktash, J.A. Cameron, M. Devlin, J. Eberth, S. Flibotte, D.S. Haslip, D.R. LaFosse, I.Y. Lee, A.O. Macchiavelli, R.W. MacLeod, J.M. Nieminen, S.D. Paul, L.L. Riedinger, D. Rudolph, D.G. Sarantites, H.G. Thomas, J.C. Waddington, W. Weintraub, J.N. Wilson, A.V. Afanasjev, and I. Ragnarsson, Phys. Rev. Lett. **79**, 1233 (1997).
[5] J. Pavan, S.L. Tabor, A.V. Afanasjev, C. Baktash, F. Cristancho, M. Devlin, J. Döring, C.J. Gross, G.D. Johns, R.A. Kaye, D.R. LaFosse, I.Y. Lee, F. Lerma, A.O. Macchiavelli, I. Ragnarsson, D.G. Sarantites, and G.Z. Solomon, Phys. Rev. C **67**, 034316 (2003).
[6] G.B. Carlsson, Master thesis, Lund Institute of Technology, 2003, Lund-MPh-03/01.
[7] M. Wiedeking, R.A. Kaye, G.Z. Solomon, S.L. Tabor, J. Döring, G.D. Johns, F. Cristancho, M. Devlin, F. Lerma, D.G. Sarantites, I.Y. Lee, and A.O. Macchiavelli, Phys. Rev. C **62**, 024316 (2000).
[8] M. Wiedeking, S.L. Tabor, F. Cristancho, M. Devlin, J. Döring, C.B. Jackson, G.D. Johns, R.A. Kaye, I.Y. Lee, F. Lerma, A.O. Macchiavelli, M. Naidu, I. Ragnarsson, D.G. Sarantites, and G.Z. Solomon, Phys. Rev. C **67**, 034320 (2003).
[9] J. Döring, Y.A. Akovali, C. Baktash, F.E. Durham, C.J. Gross, P.F. Hua, G.D. Johns, M. Korolija, D.R. LaFosse, I.Y. Lee, A.O. Macchiavelli, W. Rathbun, D.G. Sarantites, D.W. Stracener, G.Z. Solomon, S.L. Tabor, A. Vander Molen, A.V. Afanasjev, and I. Ragnarsson, Phys. Rev. C **61**, 034310 (2000).
[10] D. Galeriu, D. Bucurescu, and M. Ivasku, J. Phys. G **12**, 329 (1986).

[11] T. Bengtsson and I. Ragnarsson, Nucl. Phys. **A436**, 14 (1985).
[12] G. Andersson, S.E. Larsson, G. Leander, P. Möller, S.G. Nilsson, I. Ragnarsson, S. Åberg, R. Bengtsson, J. Dudek, B. Nerlo-Pomorska, K. Pomorski, and Z. Szymański, Nucl. Phys. **A268**, 205 (1976).
[13] S.G. Nilsson and I. Ragnarsson, *Shapes and Shells in Nuclear Structure* (Cambridge University Press, Cambridge, 1995).
[14] D. Glas, U. Mosel, and P.G. Zint, Z. Phys. A **285**, 83 (1978).
[15] V.M. Strutinsky, Nucl. Phys. **A95**, 420 (1967).
[16] S. Cohen, F. Plasil, and W.J. Swiatecki, Ann. Phys. (N.Y.) **82**, 557 (1974).
[17] P. Ring, A. Hayashi, K. Hara, H. Emling, and E. Grosse, Phys. Lett. **110B**, 423 (1982).
[18] I. Ragnarsson, V.P. Janzen, D.B. Fossan, N.C. Schmeing, and R. Wadsworth, Phys. Rev. Lett. **74**, 3935 (1995).
[19] A.V. Afanasjev and I. Ragnarsson, Nucl. Phys. **A591**, 387 (1995).
[20] M. Beiner, H. Flocard, N. Van Giai, and P. Quentin, Nucl. Phys. **A238**, 29 (1975).
[21] G.A. Lalazissis, J. König, and P. Ring, Phys. Rev. C **55**, 540 (1997).
[22] P. Federman, and S. Pittel, Phys. Rev. C **20**, 820 (1979).
[23] A. De-Shalit and M. Goldhaber, Phys. Rev. **92**, 1211 (1953).
[24] J. Dobaczewski, W. Nazarewicz, J. Skalski, and T. Werner, Phys. Rev. Lett. **60**, 2254 (1988).
[25] J. Rekstad and G. Løvhøiden, Nucl. Phys. **A267**, 40 (1976).
[26] M. Bender, K. Rutz, P.-G. Reinhard, J.A. Maruhn, and W. Greiner, Phys. Rev. C **60**, 034304 (1999).
[27] V.I. Dimitrov, F. Dönau, and S. Frauendorf, Phys. Rev. C **62**, 024315 (2000).
[28] W.D. Myers and W.J. Swiatecki, Ark. Fys. **36**, 343 (1967).
[29] I. Ragnarsson, Z. Xing, T. Bengtsson, and M.A. Riley, Phys. Scr. **34**, 651 (1986).
[30] I. Hamamoto, Phys. Lett. **102B**, 225 (1981).
[31] S.L. Tabor, J. Döring, G.D. Johns, R.A. Kaye, G.N. Sylvan, C.J. Gross, Y.A. Akovali, C. Baktash, D.W. Stracener, P.F. Hua, M. Korolija, D.R. LaFosse, D.G. Sarantites, F.E. Durham, I.Y. Lee, A.O. Macchiavelli, W. Rathbun, and A. Vander Molen, Phys. Rev. C **56**, 142 (1997).